Tenth International Conference on Computational Fluid Dynamics (ICCFD10), Barcelona, Spain, July 9-13, 2018

ICCFD10-xxxx

An improved Barth-Jesperson limiter for Flux-Reconstruction method and its applications

Zhiqiang He*, Zhongzhou Guo*, Wenwen Zhao* and Weifang Chen*
Corresponding author: wwzhao@zju.edu.cn

*College of Aeronautics and Astronautics, Zhejiang University, Hangzhou 310027, China

1 Introduction

The second-order CFD methods have been playing an important role in the design of aircraft. However, it is unable to capture structure details while solving complex unsteady flows due to the excessive dissipation introduced through the spatial discretization. At the same time, high-order methods can obtain more flow details at a lower computational cost. DG (Discontinuous Galerkin Method) is very popular these years for its ability to get arbitrary order accuracy with unstructured grids. But its huge computational cost restricts its scope of application.

Flux Reconstruction (FR) method was first introduced by Huynh in 2007 [1], which is capable to recover several high-order schemes for linear fluxes, including spectral difference (SD) and nodal discontinuous Galerkin (NDG). Not like DG, FR method employs difference equations rather than integral equations. It discretize the numerical solution through expansions using piecewise high-order Lagrange polynomial basis functions, then choose a correction polynomial, for example, Raudu polynomial, to reconstruct a globally continuous flux from the piecewise discontinuous flux in each cell. Study in paper [investigation of 3d internal flow using new flux-reconstruction high order method] show that FR is 8 times faster than DG for p1, p2 and p3. Recently, flux reconstruction method has been successfully applied to aeroacoustics [2], large eddy simulation [3, 4] and so on, and thus gain wider attention. However, there are still some issues when FR is applied in transonic and supersonic flows, where shock-capturing is still not fully satisfactory.

Artificial viscosity and limiting are two common strategies to suppress spurious non-physical oscillations around shock. One important advantage of the artificial viscosity method is that only the information of current cell is needed, so it keeps the compact of the FR method. However, such a method can potentially change the order of the equations, and thus reduce the time step. The other drawback of artificial viscosity is that it is problem-dependent. It requires some experiences to get appropriate viscosity. Otherwise, excessive viscosity will affect the precision of the solution, or too small one cannot suppress spurious non-physical oscillations. Artificial viscosity was used to capture the shock successfully at 1.6 Ma for NACA0012 airfoil in paper [5]. Limiting is widely used in FVM with much success. Limiting limits the solution to satisfy TVD or TVB properties, and can totally suppress oscillations around shocks. Since FR method is very similar to nodal DG, it would be natural to apply limiters designed for nodal DG to FR. MLP (hierarchical multi-dimensional limiting process) designed for DG was firstly introduced to FR in paper [6], which is able to capture the flow structures in detail. However, it requires wider stencils than traditional limiters for second-order CFD methods, and thus makes it more difficult to program. WENO schemes were also introduced to FR in paper [7]. It eliminates the oscillation while keeping high order accuracy. But it's quite difficult to apply it to hybrid grid solver. In this paper, we introduce an improved Barth-Jesperson limiter to FR method, and employ a shock indicator, to maintain high order accuracy in smooth regions while suppressing oscillations around shocks.

The paper is organized as follows. In the second section, the governing equations and FR method

are briefly reviewed. In the third section, shock detector and an improved Barth-Jesperson limiter are described in detail. In the final section, we draw a conclude and summarize some future works.

2 Governing equations and Flux Reconstruction method

2.1 Euler equations

The oscillations around shock will be surpassed with limiter functions. However, the solution in smooth regions will also be limited and polluted. It's essential to turn off limiter in smooth regions if we want to maintain high order accuracy. A smoothness indicator from the artificial viscosity method is employed as a shock detector [2].

The unsteady Euler equations can be written in conservative form as

$$\frac{\partial \boldsymbol{u}(x,t)}{\partial t} + \nabla \cdot \boldsymbol{F}(\boldsymbol{u}) = 0 \tag{1}$$

where conservative state vector and flux are defined as

$$\boldsymbol{u} = \begin{bmatrix} \rho \\ \rho u_i \\ e \end{bmatrix}, \boldsymbol{F} = \begin{bmatrix} \rho u_j \\ \rho u_i u_j + p\delta_{ij} \\ u_j(e+p) \end{bmatrix} \tag{2}$$

in which ρ, e, p denote density, total energy and pressure, u_i denote velocities. For a perfect gas, the pressure is given by

$$p = (\gamma - 1)(e - \frac{1}{2}\rho u_j u_i) \tag{3}$$

The specific heat ratio is assumed to be constant and equals to 1.4.

2.2 Flux Reconstruction method

Consider 1D hyperbolic law

$$\frac{\partial u(x,t)}{\partial t} + \frac{\partial F(u)}{\partial x} = 0 \tag{4}$$

Firstly, discrete the computational domain $\Omega = [x_0, x_N]$ into N non-overlapping elements, $\Omega_i = [x_n, x_{n+1}], n = 0,1,\cdots,N-1$. We transform each element Ω_i to transformed space $\Omega_s = [-1,1]$ for both mathematical simplicity and computational efficiency. For 1D, mapping function for each element is

$$x = \theta(\xi) = \frac{1-\xi}{2}x_n + \frac{1+\xi}{2}x_{n+1} \tag{5}$$

The governing equation Eq(4) in transformed space becomes

$$\frac{\partial \hat{u}}{\partial t} + \frac{1}{J_i}\frac{\partial \hat{F}}{\partial \xi} = 0 \tag{6}$$

where, $\hat{u} = u(\Theta_i(\xi), t), \hat{F} = F(\Theta_i(\xi), t), J_i = \left.\frac{\partial x}{\partial \xi}\right|_{\Omega_i}$.

Then, define $k+1$ solution points in Ω_s, so the solution $\hat{u}_i^\delta$ and flux $\hat{F}_i^\delta$ can be approximated by following K-th order Lagrange interpolate polynomials

$$\begin{aligned} \hat{u}^\delta &= \sum_{i=0}^{k+1} \hat{u}_i^\delta l_i(\xi) \\ \hat{F}^{\delta D} &= \sum_{i=0}^{k+1} \hat{F}_i^\delta l_i(\xi) \end{aligned} \tag{7}$$

where $l_i(\xi)$ is Lagrange interpolate basis defined at solution points in Ω_s. The flux $\hat{F}_i^\delta$ is generally

discontinuous across cell interfaces. To satisfy the conservation law, correction functions g_L and g_R were introduced to keep the flux continuous at cell interfaces. VCHJ correction functions are the most frequently used correction functions [8]. They are

$$g_L = \frac{(-1)^k}{2}\left[L_k - \left(\frac{\eta_k L_{k-1} + L_{k+1}}{1+\eta_k}\right)\right]$$
$$g_R = \frac{1}{2}\left[L_k + \left(\frac{\eta_k L_{k-1} + L_{k+1}}{1+\eta_k}\right)\right] \tag{8}$$

where L_k is the Legendre polynomial of degree p and

$$\eta_k = \frac{c(2k+1)(a_k k!)^2}{2} \tag{9}$$

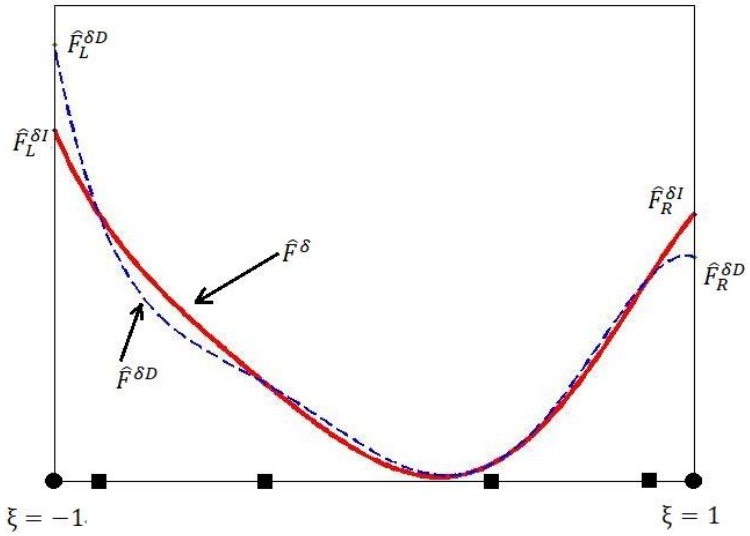

Figure 1. Figure shows the flux correction procedure in computational domain.

The parameter c is called the VCJH parameter and we can recover several existing schemes with specific c, such as nodal DG, SD. The total continuous flux is written as

$$\hat{F}^{\delta} = \hat{F}^{\delta C} + \hat{F}^{\delta D} = \sum_{i=0}^{k} \hat{F}_i^{\delta} l_i(\xi) + \left(\hat{F}_L^{\delta I} - \hat{F}_L^{\delta D}\right) g_L + \left(\hat{F}_R^{\delta I} - \hat{F}_R^{\delta D}\right) g_R \tag{10}$$

where $\hat{F}^{\delta C}$ is correction component of the continuous flux,

$$\hat{F}^{\delta C} = \left(\hat{F}_L^{\delta I} - \hat{F}_L^{\delta D}\right) g_L + \left(\hat{F}_R^{\delta I} - \hat{F}_R^{\delta D}\right) g_R \tag{11}$$

$\hat{F}_L^{\delta I}$ and $\hat{F}_R^{\delta I}$ are fluxes at left and right interfaces computed with Riemann solver, $\hat{F}_L^{\delta D}$ and $\hat{F}_R^{\delta D}$ are discontinuous fluxes at cell boundary. The derivative of the continuous flux is

$$\frac{\partial \hat{F}^{\delta}}{\partial \xi}(\xi_i) = \sum_{i=0}^{k} \hat{F}_i^{\delta} \frac{dl_i(\xi)}{d\xi}(\xi_i) + \left(\hat{F}_L^{\delta I} - \hat{F}_L^{\delta D}\right) \frac{dg_L}{d\xi}(\xi_i) + \left(\hat{F}_R^{\delta I} - \hat{F}_R^{\delta D}\right) \frac{dg_R}{d\xi}(\xi_i) \tag{12}$$

Finally, Eq(12) is used in Eq(6) to obtain an ODE which is then time-advanced using a high-order time integration scheme, like RK45 in this paper.

3 Shock detector and an improved Barth-Jesperson limiter

3.1 Shock detector

The oscillations around shock will be surpassed with limiter functions. However, the solution in smooth regions will also be limited. It's essential to turn off limiter in the smooth regions if we want to maintain high order accuracy. A smoothness indicator from the artificial viscosity method is employed as shock detector [9].

Firstly, compute the L_2 projection to the lower-order space of the k-th order solution in cell i.

$$\hat{u} = \sum_{i=0}^{k} u_i L_i \tag{13}$$

Next, define smoothness indicator S_e as

$$S_e = \log_{10} \frac{\int_e |u - \hat{u}|^2 \, de}{\int_e |u|^2 \, de} \tag{14}$$

After that, we introduce σ_i,

$$\sigma_i = \begin{cases} 1 & S_i < S_0 - \kappa \\ \frac{1}{2}\left(1 - sin\left(\frac{\pi}{2}\frac{S_e - S_0}{\kappa}\right)\right) & S_0 - \kappa \le S_i < S_0 + \kappa \\ 0 & S_i \ge S_0 + \kappa \end{cases} \tag{15}$$

where $\kappa = 4, S_0 = -C_0 log(k), C_0 = 3$. Finally, if $\sigma_i < 0.99$, the cell is identified as a "trouble cell", and its solutions are going to be limited.

3.2 An improved Barth-Jesperson limiter for FR

As mentioned in section 2.2, the solution in cell is a polynomial in the form Eq(7). The Gibb's phenomenon would cause oscillations around shock and unphysical solutions. An improved Barth-Jesperson limiter is introduced to FR method to avoid this at the average step. All steps required are listed below as

1) Find all "trouble cells" with the help of shock detector mentioned in last section.
2) Evaluate the average solutions of "trouble cells" and their neighbors sharing a face, $\bar{u}_i$ and $\bar{u}_{nb}$.
3) Find the maximum average value $\bar{u}_{\max}$ and minimum average value $\bar{u}_{\min}$ among "trouble cell" and its neighbors.
4) Evaluate average gradient, $\overline{\nabla u_i}$ of "trouble cell".
5) For cell i, define a limiter function

$$\Phi_i = \min_{cr} \begin{cases} \min\left(1, \frac{\bar{u}_{\max} - \bar{u}_i}{\Delta_2}\right) & \Delta_2 > 0 \\ 1 & \Delta_2 = 0 \\ \min\left(1, \frac{\bar{u}_{\min} - \bar{u}_i}{\Delta_2}\right) & \Delta_2 < 0 \end{cases} \tag{16}$$

where $\Delta_2 = \overline{\nabla u_i} \cdot \Delta\vec{r}_{i,cr}$, $\Delta\vec{r}_{i,cr}$ is the vector from cell center to cell corner.

6) Limit the solution at solution points

$$u_{i,j} = \bar{u}_i + \Phi_i \overline{\nabla u_i} \bullet \Delta\vec{r}_{i,j} \tag{17}$$

7) The limited solution is then used in FR procedure.

We use cell corner to avoid evaluating solution at every flux point. Step 6 shows that solution at "trouble cell" is linearly distributed so all solutions at solution points and flux points have the TVD property.

4 Numerical results

4.1 1D sod shock tube problem

The sod shock tube problem is a common one-dimensional Riemann problem to test for the accuracy of computational fluid codes. The test can be described with Euler equation with following parameters, for left and right states of an ideal gas

$$(\rho, u, p) = \begin{cases} (1.0, 0.0, 1.0) & 0 \le x \le 0.5 \\ (0.125, 0, 0.1) & 0.5 < x \le 1.0 \end{cases}. \quad (18).$$

The simulation is stopped at t=0.2 and with 100, 200 and 400 elements. The density distribution computed with third-order FR scheme with shock detector and the improved Barth-Jesperson limiter is shown in Figure 2.

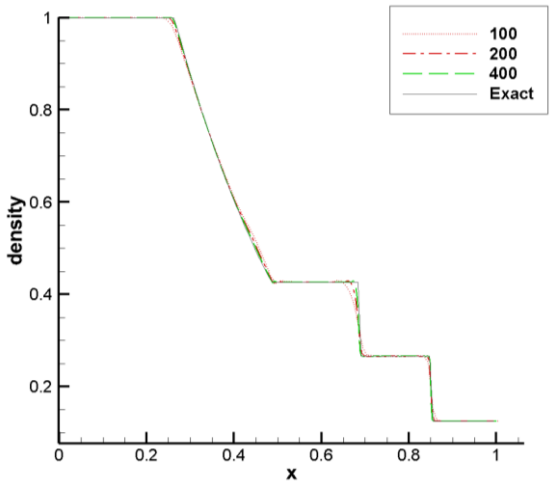

Figure 2: Density distribution with different elements at t=0.2s

4.1 Supersonic flow in a convergent nozzle with a ramp

The case is to test limiter for steady problem. Its computational domain and boundary conditions are shown in Figure 3. The initial conditions are as follows:

$$\rho = 1.4, u = 2.0, v = 0, p = 1.0$$
$$i.e., Ma = 2.0 \quad (19).$$

The velocity of supersonic inflow is also 2.0 Mach. Both structured and unstructured grids are employed. The density distributions computed with fourth order FR scheme with shock detector and the improved Barth-Jesperson limiter are shown in Figure 4. The shock captured here is very sharp and almost no overshot. It shows that the improved limiter here inherits advantages of Barth-Jesperson limiter in second-order FVM, and is able to function for both structured and unstructured grids.

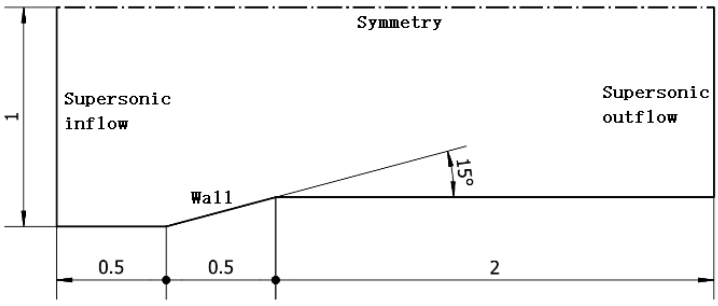

Figure 3: Computational domain and boundary conditions of convergent nozzle problem.

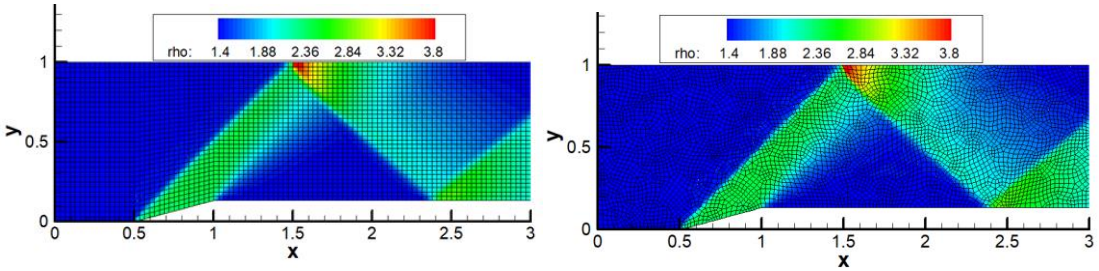

Figure 4: Density distribution of convergent nozzle problem with structured and unstructured grids.

4.3 Mach 3 wind tunnel with a forward step

In this section, a standard test case is simulated to evaluate FR schemes with the improved limiter. The problem contains a supersonic Mach 3 uniform inflow in a wind tunnel with a forward step, multiple interactions of shocks, expansion fans and contact discontinuities. The computational domain and boundary conditions are shown in Figure 1. And a set of h=1/160 quadrilateral grids is employed. The initial conditions are listed as follows:

$$\rho = 1.4, u = 3.0, v = 0, p = 1.0, Ma = 3.0 \quad (20).$$

Figure 2 and Figure 3 show the shock sensor and density distributions at t=4.0s computed with the third and the fourth order FR scheme with the improved limiter. Both shock sensors capture flow structures accurately and the higher order scheme yields more detailed features. The test case also validates the resolving capability of the improved Barth-Jesperson limiter for the Kelvin-Helmholtz instability from the shock triple point, which indicates that FR scheme with the new limiter is of low dissipation.

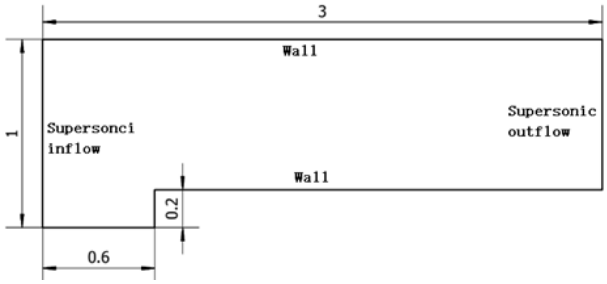

Figure 5: Computational domain and boundary conditions of the forward step

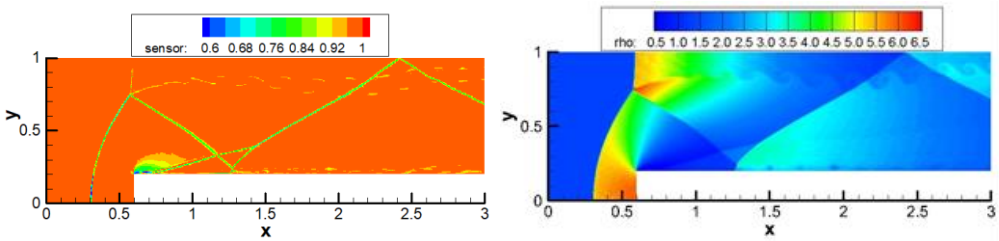

Figure 6: Shock sensor and density distribution for the 3rd order FR scheme at t=4s.

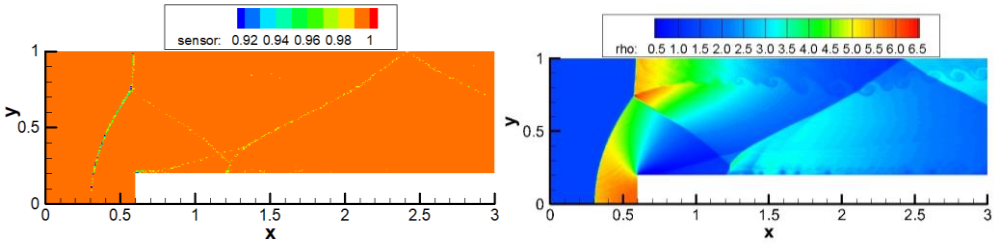

Figure 7: Shock sensor and density distribution for 4th order FR scheme at t=4s.

5 Conclusion

An improved Barth-Jesperson limiter for FR scheme is developed in this paper. It keeps stencils

of the original Barth-Jesperson limiter for the second-order FVM scheme, and thus is easy to realize based on FVM codes. Some test cases are carried out up to examine the capability of the improved limiter in capturing supersonic flow physics. Results demonstrate the proposed limiter provides detailed flow structures without oscillations around shock region, and maintains the required accuracy in smooth region at the same time.

References

[1] Huynh H T. A flux reconstruction approach to high-order schemes including discontinuous Galerkin methods. AIAA paper, 2007-4079: 2007.

[2] Visbal M R, Gaitonde D V. Very high-order spatially implicit schemes for computational acoustics on curvilinear meshes. Journal of Computational Acoustics, 2001, 9(04): 1259-1286.

[3] Lu Y, Liu K, Dawes W N. Large eddy simulations using high order flux reconstruction method on hybrid unstructured meshes//AIAA Science and Technology Forum and Exposition (SciTech2014), AIAA2014-0424. 2014.

[4] Park J S, Witherden F D, Vincent P E. High-Order Implicit Large-Eddy Simulations of Flow over a NACA0021 Aerofoil. AIAA Journal, 2017.

[5] Lopez-Morales M, Bull J, Crabill J, et al. Verification and Validation of HiFiLES: a High-Order LES unstructured solver on multi-GPU platforms. AIAA Paper, 2014, 3168.

[6] Park J S, Chang T K, Kim C. Higher-order multi-dimensional limiting strategy for correction procedure via reconstruction[C]//52nd Aerospace Science Meeting. 2014: 2014-0772.

[7] Du J, Shu C W, Zhang M. A simple weighted essentially non-oscillatory limiter for the correction procedure via reconstruction (CPR) framework. Applied Numerical Mathematics, 2015, 95: 173-198.

[8] Vincent P E, Castonguay P, Jameson A. A new class of high-order energy stable flux reconstruction schemes. Journal of Scientific Computing, 2011, 47(1): 50-72.

[9] Persson P O, Peraire J. Sub-cell shock capturing for discontinuous Galerkin methods. AIAA paper, 2006-0112: 2006.